Journal of Statistics Applications & Probability
An International Journal

http://dx.doi.org/10.18576/jsap/150603

A New Class of Distributions: Formulation, Statistical Properties and Applications

Reem Taha Abdulqader[1], *Rana H. Khashab*[2,*], *Mundher A. Khaleel*[1], *Said G. Nassr*[3], *Ghareeb A. Marei*[4], *and Mohammed Elgarhy*[4,5]

[1]Mathematics Departments, College of Computer Science and Mathematics, Tikrit University, Iraq
[2]Mathematics Department, Faculty of Sciences, Umm Al-Qura University, Makkah, Saudi Arabia
[3]Department of Statistics and Insurance, Faculty of Commerce, Arish University, El-Arish 45511, Egypt
[4]Faculty of Computers and Information Systems, Egyptian Chinese University, Nasr City, Egypt
[5]Department of Computer Engineering, Biruni University, 34010 Istanbul, Turkey

Received: 5 Jun. 2026, Revised: 2 Aug. 2026, Accepted: 14 Oct. 2026
Published online: 1 Nov. 2026

Abstract: In this paper we present a general Spliced-Bridge class of continuous distributions where a central distribution is connected to two tail regions through a CDF-based rescaling approach. We propose construction that maintains continuity and treats the two breakpoints as unknown model parameters. We consider the Exponential-Weibull-Exponential (EWE) model for which several distributional and reliability properties are obtained, including moments, survival, hazard, cumulative hazard, reversed hazard and quantile functions. We explore different estimation methods, including maximum likelihood, least squares, weighted least squares, Cramér-von Mises, Anderson-Darling, maximum product spacings, percentile matching and quantile least squares. We demonstrate that our Monte Carlo studies with sample sizes n=20,50,125 and 250 are much more accurate as the sample size increases. Percentile matching is most effective for small samples, while maximum likelihood is the most efficient overall estimator for moderate and large samples. Application to glass-fiber strength data shows the flexibility of the EWE model, which is the best relative fit among all the competing models according to the main information and goodness of fit criteria. The proposed Spliced-Bridge framework thus offers a more flexible and interpretable way to model data with different central and tail behaviors.

Keywords: spliced-Bridge Class; Exponential-Weibull-Exponential distribution; heavy tails; goodness-of-fit criteria

1 Introduction

Flexible probability distributions are a very important concern in modern statistical modeling because many empirical data sets have structural features that cannot be adequately modeled by a classical one- or two-parameter model. Skewness, excess kurtosis, tail asymmetry, multimodality, change in hazard behavior and heterogeneous failure mechanisms are common phenomena in reliability, survival, actuarial, environmental, financial and biomedical fields. The field of distributions has been rapidly developing a family of generalized distributions in which additional parameters or transformation algorithms are introduced to increase shape flexibility while retaining the distribution function to be mathematically tractable. These early developments include the Marshall-Olkin parameter extension mechanism [28], beta-generated construction as shown in the beta-normal model [20], Kumaraswamy-G family [15], and T-X method for continuous distribution generation [11].

Literature has expanded in many directions. Recent works have proposed new two-parameter models, heavy-tailed distributions, trigonometric extensions, generalized exponential extensions, inverse Rayleigh-based developments, skewness-reducing transformations, neutrosophic extensions and transformed-X families [1, 10, 13, 19, 21, 22, 27, 30–32, 35, 36]. In addition, the exponentiated generalized Topp-Leone-G family [35], generalized flexible families and Marshall-Olkin-Lomax extensions [3, 23], and generalized odd Frechet-exponentiated-G constructions [2] are all proposed. Further recent lifetime models include extended Lindley,

* Corresponding author e-mail: rhkhashab@uqu.edu.sa

© 2026 NSP
Natural Sciences Publishing Cor.

one-parameter decreasing-hazard and odds-based Weibull distributions [5, 24, 33]. In general, the new models show that more shape parameters, generators and transformations are possible to make probability distributions more flexible to model the density, survival and hazard-rate of different situations. However, the rising complexity of such families also highlights a major issue of the method in general: more flexibility does not come at the cost of not being interpretable, of having unstable inference, or of having too complicated analytical forms.

The practical motivation for flexible models is also strong. The applications are financial and interactive-data analysis [27], heavy-tailed real-data modeling [21], lifetime and environmental data [10], medical and health-related data [1, 6, 32, 38], reliability and engineering problems [22, 29, 31, 39], and survival analysis in cancer studies [25]. Reliability inference for such models under progressive, hybrid, step-stress and record-based schemes, including stress-strength reliability, has also been developed [4, 7–9, 18, 34]. These are often examples where one global distributional mechanism is not suitable. For example, the behavior of the central mass may be very different from the lower and upper tails and the failure mechanism may change across different parts of the support. These features suggest that a good model should allow for the tails and central region to be controlled separately with the same probability structure. In addition to the model construction, reliable estimation and goodness-of-fit assessment are key to determining if the extra flexibility is statistically significant. Classical and modern approaches based on empirical-distribution discrepancies like Cramer-von Mises and Anderson-Darling principles [12, 16] and quasi-linear and percentile-based approaches [17, 40] are also used to evaluate the accuracy of estimators and model adequacy. This is particularly relevant for highly parameterized or piecewise models, where likelihood surfaces are not smooth and different estimation methods may respond differently to the tail behavior, central concentration and transition point. Another line of research is based on composite and spliced distributions. Composite models are those that join different component distributions at one or more thresholds and have been used in loss modeling and heavy-tail models [14, 26, 37]. However, many classical composite constructions assume continuity (and sometimes differentiability) at the density level. This means that the threshold may be found by matching constraints rather than estimated from the data, and the results can be cumbersome to analyze. For example, standard splicing approaches also typically assign separate component distributions to disjoint intervals and do not introduce a flexible central transition mechanism. This limits construction that retains the intuitive benefits of splicing but allows the transition region itself to be modeled and estimated.

Motivated by these considerations, this paper introduces a general class of continuous distributions, called Spliced-Bridge. The construction is directly in the CDF space. A simple base distribution F1 accounts for the two tails and a second one F2 for a bridge across the interval (a, b). The bridge CDF is linearly rescaled so that it is the same as the boundary value of F1 at the two breakpoints. This way the total CDF is continuous, the piecewise density is simple, and the breakpoints a and b are free model parameters. Thus, the proposed class separates tail behavior, central mass shape and transition location effects in a transparent and interpretable manner. The main contributions of this work are:

1. We have developed and studied the Spliced-Bridge family rigorously and shown the validity and basic properties of its CDF and PDF construction.
2. We have developed and studied the Exponential-Weibull-Exponential (EWE) sub-model in which exponential tails are connected via a Weibull bridge and derive its most important distributional properties such as moments, survival, hazard, cumulative-hazard, reversed-hazard, quantile, entropy and so on.
3. To investigate parameter estimation when the breakpoints are unknown and to compare several estimation methods with an extensive Monte Carlo study using bias, MSE, RMSE, MAE, dispersion, convergence behavior and composite ranking criteria.
4. To evaluate the empirical usefulness of the proposed model by real data analysis and comparative to other flexible distributions with likelihood-based information criteria and goodness-of-fit measures.
5. To provide a simple framework that can be extended by replacing the tail or bridge distribution and generate a large collection of interpretable sub-models for reliability, survival, actuarial, financial, environmental, etc.

The rest of the paper is organized as follows. In section 2 we define the Spliced-Bridge family formally, its interpretation and special cases and typical sub-models. In section 3 we develop the main distribution properties of the EWE model. We discuss statistical inference and the simulation study in section 4. The real data analysis and comparison in the next section is followed by our main conclusions and further work.

2 The Spliced-Bridge Family

2.1 Definition

Let F_1 and F_2 be absolutely continuous CDFs defined on $\mathbb{R}$ with corresponding densities f_1 and f_2. Choose real numbers $a < b$ such that $F_2(b) > F_2(a)$. The spliced-bridge CDF is defined by:

© 2026 NSP
Natural Sciences Publishing Cor.

$$F(x) = \begin{cases} F_1(x), & x \le a, \\ F_1(b) + \frac{F_1(b)-F_1(a)}{F_2(b)-F_2(a)} \left(F_2(x) - F_2(b)\right), & a < x \le b, \\ F_1(x), & x > b. \end{cases} \tag{1}$$

The construction can be interpreted as follows. The left tail (-∞, a] and the right tail (b, ∞) follow exactly the distribution F_1. In the central region (a, b], the CDF is a linear function of F_2, rescaled to match the boundary values $F(a) = F_1(a)$ and $F(b) = F_1(b)$. Because F_2 is non-decreasing on [a, b] (and its endpoint increment is positive since $F_2(b) > F_2(a)$), the middle piece is non-decreasing, and the whole function is continuous. The limits as $x \to -\infty$ and $x \to \infty$ are 0 and 1 respectively because F_1 is a proper CDF. Hence F is a valid continuous CDF.

Differentiating (1) almost everywhere yields the probability density function (PDF)

$$f(x) = \begin{cases} f_1(x), & x < a, \\ \frac{F_1(b)-F_1(a)}{F_2(b)-F_2(a)} f_2(x), & a < x < b, \\ f_1(x), & x > b. \end{cases} \tag{2}$$

At the breakpoints $x = a$ and $x = b$ the density need not be defined; they contribute zero probability. The normalizing constant $\beta = [F_1(b) - F_1(a)] / [F_2(b) - F_2(a)]$ guarantees

$$\int_{-\infty}^{\infty} f(x)\, dx = 1.$$

The family is extremely flexible because:

–F_1 controls the tail behaviour (e.g., exponential, Pareto).
–F_2 shapes the central mass, which can accommodate skewness, multimodality, or high kurtosis.
–The breakpoints a and b are free parameters that determine the extent of the bridge; they can be estimated from data.

2.2 Special and limiting cases

–If $a \to -\infty$ or $b \to \infty$, the bridge disappears and the model reduces to F_1 everywhere.
–If $a = b$, the middle interval vanishes and the distribution becomes exactly F_1.
–If F_1 and F_2 are the same distribution, the CDF reduces to F_1 for all x.
–Many two-component composite models can be seen as a special case where the bridge is degenerate (no scaling) and the breakpoint is fixed by continuity.

2.3 Sub-models of interest

Several sub-models are obtained by choosing specific F_1 and F_2 from standard families. Table 1 lists a few. For the remainder of this paper we focus on the Exponential–Weibull–Exponential (EWE) model, where F_1 is the exponential CDF with rate λ and F_2 is the Weibull CDF with shape k and scale θ. The CDF and PDF simplify as

$$F_{EWE}(x) = \begin{cases} 1 - e^{-\lambda x}, & x \le a, \\ 1 - e^{-\lambda b} + \frac{e^{-\lambda a} - e^{-\lambda b}}{F_2(b)-F_2(a)} \left(F_2(x) - F_2(b)\right), & a < x \le b, \\ 1 - e^{-\lambda x}, & x > b, \end{cases} \tag{3}$$

$$f_{EWE}(x) = \begin{cases} \lambda e^{-\lambda x}, & x < a, \\ \frac{e^{-\lambda a} - e^{-\lambda b}}{F_2(b)-F_2(a)} \frac{k}{\theta} \left(\frac{x}{\theta}\right)^{k-1} e^{-(x/\theta)^k}, & a < x < b, \\ \lambda e^{-\lambda x}, & x > b, \end{cases} \tag{4}$$

where $F_2(t) = 1 - e^{-(t/\theta)^k}$. This model has five unknown parameters: $\lambda > 0$, $k > 0$, $\theta > 0$, and the breakpoints $a < b$. The EWE expressions apply on $x \ge 0$, with $0 < a < b$. For $x < 0$, set F_EWE(x) = 0 and f_EWE(x) = 0. The five parameters are (λ, k, θ, a, b), and β denotes the CDF-bridge scaling factor.

Figure 1 represents the plot of the CDF and pdf functions, the EWE distribution, and different sets of parameter values.

Figure 1 shows the flexibility of the EWE distribution. The CDF increases smoothly toward one while the PDF exhibits noticeably different shapes as the parameters vary– the model is able to represent different levels of concentration and skewness in the bridge region.

© 2026 NSP
Natural Sciences Publishing Cor.

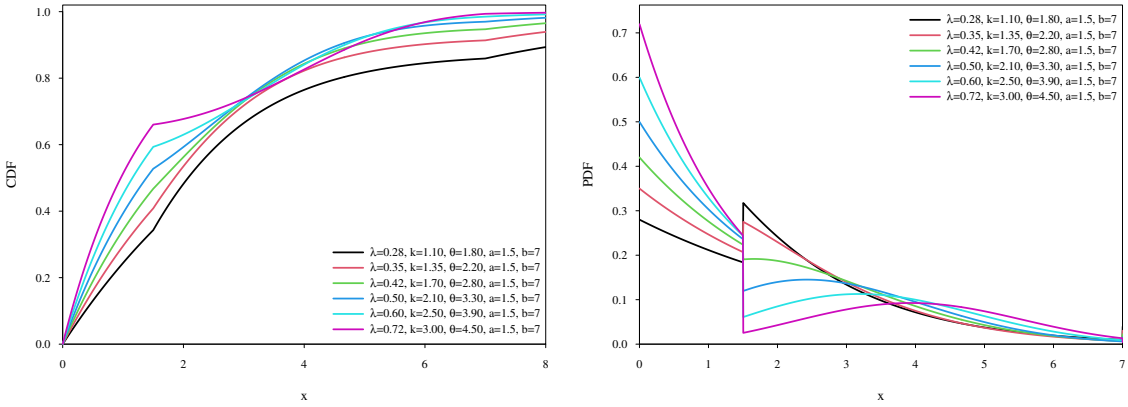

Fig. 1: EWE cumulative distribution (A) and density (B) for five illustrative parameter configurations. Reference: (λ, k, θ, a, b) = (0.5, 2, 3, 2, 6); alternatives vary λ or k as indicated in the legend. Dotted vertical guides show the breakpoints.

2.4 Survival and Related Reliability Functions of the EWE Distribution

For the Exponential-Weibull-Exponential (EWE) sub-model, the exponential distribution controls the two tail regions, while the Weibull distribution controls the central bridge over the interval (a,b). Let

$$F_2(x) = 1 - exp\left[-\left(\frac{x}{\theta}\right)^k\right],$$

and

$$f_2(x) = \frac{k}{\theta}\left(\frac{x}{\theta}\right)^{k-1} \exp\left[-\left(\frac{x}{\theta}\right)^k\right].$$

The bridge scaling constant is

$$\beta = \frac{F_1(b) - F_1(a)}{F_2(b) - F_2(a)} = \frac{e^{-\lambda a} - e^{-\lambda b}}{F_2(b) - F_2(a)}.$$

Using the EWE cumulative distribution function and probability density function, the principal reliability functions are obtained as follows.

2.4.1 Survival Function

The survival function is defined by

$$S(x) = 1 - F(x).$$

Hence, for the EWE distribution,

$$S_{EWE}(x) = \begin{cases} e^{-\lambda x}, & 0 \le x \le a, \\ e^{-\lambda b} + \beta\left[F_2(b) - F_2(x)\right], & a < x \le b, \\ e^{-\lambda x}, & x > b, \end{cases} \tag{5}$$

Equivalently, the middle expression may be written as $e^{-\lambda b} + \beta\left[F_2(b) - F_2(x)\right]$.

© 2026 NSP
Natural Sciences Publishing Cor.

2.4.2 Hazard Rate Function

The hazard rate function is

$$h(x) = \frac{f(x)}{S(x)}.$$

Therefore,

$$h_{EWE}(x) = \begin{cases} \lambda, & 0 < x < a, \\ \frac{\beta f_2(x)}{e^{-\lambda b} + \beta [F_2(b) - F_2(x)]}, & a < x < b, \\ \lambda, & x > b, \end{cases} \tag{6}$$

Thus, the hazard rate is constant in both exponential tails and may exhibit a wide variety of shapes within the Weibull bridge, depending mainly on k and θ.

2.4.3 Cumulative Hazard Function

The cumulative hazard function is defined by

$$H(x) = -\ln S(x)$$

For the EWE distribution,

$$H_{EWE}(x) = \begin{cases} \lambda x, & 0 \le x \le a, \\ -\ln\left(e^{-\lambda b} + \beta\left[F_2(b) - F_2(x)\right]\right), & a < x \le b, \\ \lambda x, & x > b, \end{cases} \tag{7}$$

Because $H(x) = -lnS(x)$, this function is non-decreasing over the support whenever the EWE model is valid.

2.4.4 Reversed Hazard Rate Function

The reversed hazard rate function is defined by

$$r(x) = \frac{f(x)}{F(x)}.$$

Accordingly,

$$r_{EWE}(x) = \begin{cases} \frac{\lambda e^{-\lambda x}}{1 - e^{-\lambda x}}, & 0 < x < a, \\ \frac{\beta f_2(x)}{1 - e^{-\lambda b} + \beta [F_2(x) - F_2(b)]}, & a < x < b, \\ \frac{\lambda e^{-\lambda x}}{1 - e^{-\lambda x}}, & x > b. \end{cases} \tag{8}$$

These expressions provide the mathematical basis for the survival, hazard, cumulative hazard and reversed hazard curves in Figures 2 and 3. The two exponential tails preserve a constant ordinary hazard rate with λ, whereas the Weibull bridge gives us the flexibility to create decreasing, increasing, unimodal, or even non-constant hazard patterns along the central region.

Figure 2 compares the survival and hazard functions. The survival probability decreases from one toward zero. The hazard equals λ in each exponential tail, while the bridge can produce an increasing, decreasing or non-monotone hazard. Figure 3 shows the cumulative hazard $H(x) = -\ln S(x)$, which must be non-decreasing, and the reversed hazard $r(x) = f(x)/F(x)$. The two transition points may generate jumps in the hazard and reversed hazard, although the CDF and survival function remain continuous.

© 2026 NSP
Natural Sciences Publishing Cor.

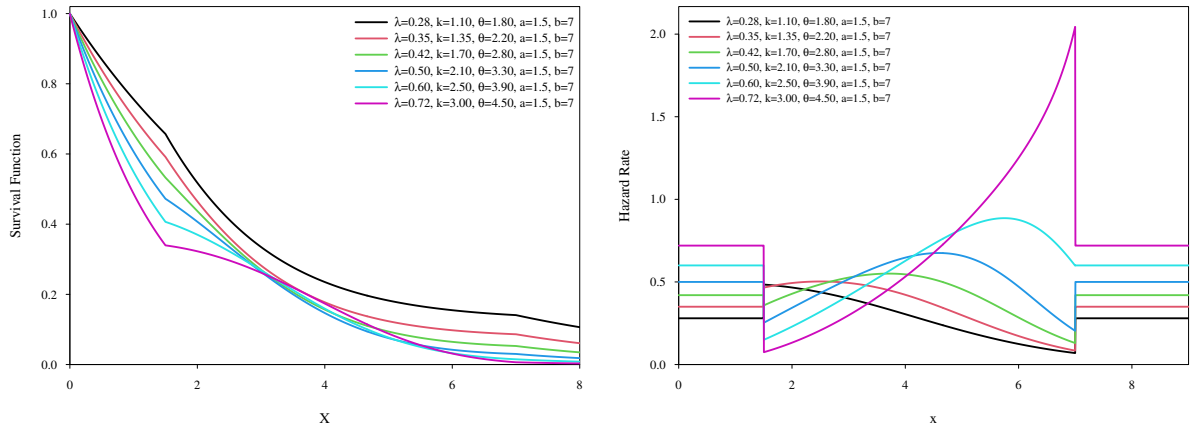

Fig. 2: EWE survival (A) and ordinary hazard (B) using the five parameter configurations defined in Figure 1. Exponential tails have constant hazard λ; the bridge hazard depends on the Weibull parameters.

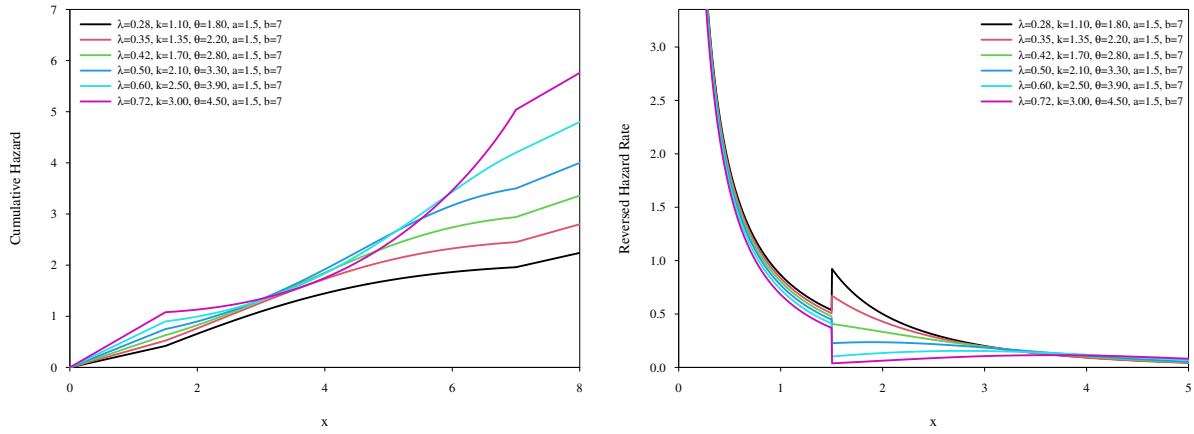

Fig. 3: EWE cumulative hazard (A) and reversed hazard (B) using the five parameter configurations defined in Figure 1. The reversed-hazard display is capped at 3.5 for readability near zero.

Table 1: Some spliced-bridge sub-models.

F_1 (tail)	F_2 (bridge)	Parameters
Exponential	Weibull	λ, k, θ, a, b
Gamma	Lognormal	shape, rate, μ, σ, a, b
Weibull	Burr	shape, scale, c, d, a, b
Lomax	Dagum	$\alpha, \beta, \gamma, a, b$

© 2026 NSP
Natural Sciences Publishing Cor.

3 Distributional Properties

We now derive mathematical properties of the spliced-bridge family, primarily using the EWE sub-model for illustration. Similar derivations apply to other choices.

3.1 Moments

The moments of the Spliced-Bridge family follow directly from its piecewise density. For any $r > 0$, the r-th raw moment is

$$E(X^r) = \int_{-\infty}^{a} x^r f_1(x)\,dx + \beta \int_a^b x^r f_2(x)\,dx + \int_b^{\infty} x^r f_1(x)\,dx. \tag{9}$$

where

$$\beta = \frac{F_1(b) - F_1(a)}{F_2(b) - F_2(a)}.$$

For the Exponential-Weibull-Exponential (EWE) model,

$$f_1(x) = \lambda e^{-\lambda x}, \qquad f_2(x) = \frac{k}{\theta}\left(\frac{x}{\theta}\right)^{k-1} \exp\left[-\left(\frac{x}{\theta}\right)^k\right].$$

Therefore,

$$E(X^r) = \int_0^a x^r \lambda e^{-\lambda x}\,dx + \beta \int_a^b x^r \frac{k}{\theta}\left(\frac{x}{\theta}\right)^{k-1} e^{-(x/\theta)^k}\,dx + \int_b^{\infty} x^r \lambda e^{-\lambda x}\,dx.$$

Using $t = \lambda x$ for the exponential parts and $u = (x/\theta)^k$ for the Weibull bridge gives

$$\int_0^a x^r \lambda e^{-\lambda x}\,dx = \lambda^{-r}\gamma(r+1, \lambda a),$$

$$\int_b^{\infty} x^r \lambda e^{-\lambda x}\,dx = \lambda^{-r}\Gamma(r+1, \lambda b),$$

and

$$\int_a^b x^r \frac{k}{\theta}\left(\frac{x}{\theta}\right)^{k-1} e^{-(x/\theta)^k}\,dx = \theta^r\left[\gamma\left(1+\frac{r}{k}, \left(\frac{b}{\theta}\right)^k\right) - \gamma\left(1+\frac{r}{k}, \left(\frac{a}{\theta}\right)^k\right)\right].$$

Hence, an equivalent compact expression for the r-th raw moment is

$$E(X^r) = \lambda^{-r}[\gamma(r+1, \lambda a) + \Gamma(r+1, \lambda b)] + \beta\theta^r\left[\gamma\left(1+\frac{r}{k}, \left(\frac{b}{\theta}\right)^k\right) - \gamma\left(1+\frac{r}{k}, \left(\frac{a}{\theta}\right)^k\right)\right]. \tag{10}$$

In particular, setting $r = 1$ yields the mean

$$E(X) = \frac{1}{\lambda}\left[1 - e^{-\lambda a}(1+\lambda a) + e^{-\lambda b}(1+\lambda b)\right] + \beta\theta\left[\gamma\left(1+\frac{1}{k}, \left(\frac{b}{\theta}\right)^k\right) - \gamma\left(1+\frac{1}{k}, \left(\frac{a}{\theta}\right)^k\right)\right]. \tag{11}$$

The second raw moment is

$$E(X^2) = \frac{1}{\lambda^2}[\gamma(3, \lambda a) + \Gamma(3, \lambda b)] + \beta\theta^2\left[\gamma\left(1+\frac{2}{k}, \left(\frac{b}{\theta}\right)^k\right) - \gamma\left(1+\frac{2}{k}, \left(\frac{a}{\theta}\right)^k\right)\right]. \tag{12}$$

Consequently,

$$Var(X) = E(X^2) - [E(X)]^2.$$

Here,

© 2026 NSP
Natural Sciences Publishing Cor.

$$\gamma(s,z) = \int_0^z t^{s-1} e^{-t}\, dt$$

is the lower incomplete gamma function, whereas

$$\Gamma(s,z) = \int_z^\infty t^{s-1} e^{-t}\, dt$$

is the upper incomplete gamma function. Thus, the moments and their derivation are presented within one unified section rather than as two separate parts.

3.2 Quantile function

The quantile function $Q(p) = F^{-1}(p)$ is obtained by solving $F(x) = p$ piecewise. For $p \le F_1(a)$, the solution is the exponential quantile $-\frac{1}{\lambda}\ln(1-p)$. For $F_1(a) < p \le F_1(b)$, we solve

$$\beta\left(F_2(x) - F_2(b)\right) = p - F_1(b) \tag{13}$$

for x, i.e., $x = Q_2\left(F_2(b) + (p - F_1(b))/\beta\right)$, where Q_2 is the Weibull quantile function. For $p > F_1(b)$, we again use the exponential quantile. This explicit representation allows easy random number generation by the inversion method.

3.3 Entropy

The Shannon entropy $-\int f(x) ln f(x)\, dx$ of the spliced-bridge distribution can be decomposed into three integrals. For the EWE model, using the piecewise PDF, we obtain

$$H = -\int_0^a \lambda e^{-\lambda x} \ln\left(\lambda e^{-\lambda x}\right) dx - \beta \int_a^b f_2(x) \ln\left(\beta f_2(x)\right) dx - \int_b^\infty \lambda e^{-\lambda x} \ln\left(\lambda e^{-\lambda x}\right) dx. \tag{14}$$

The exponential tail parts simplify to $1 - ln\lambda$, while the bridge integral can be expressed using the digamma function and the moments of the truncated Weibull distribution.

4 Statistical Inference

Let $X_1, \ldots, X_n$ be a random sample from the Exponential-Weibull-Exponential (EWE) Spliced-Bridge distribution and let $\psi = (\lambda, k, \theta, a, b)^{\mathsf{T}}, \quad \lambda > 0,\ k > 0,\ \theta > 0,\ a > 0,\ b > a$. For convenience, define

$$z_x = \left(\frac{x}{\theta}\right)^k, \qquad E_x = e^{-z_x}, \qquad R_x = e^{-\lambda x},$$

so that

$$F_1(x) = 1 - R_x, \qquad f_1(x) = \lambda R_x,$$

and

$$F_2(x) = 1 - E_x, \qquad f_2(x) = \frac{k}{\theta}\left(\frac{x}{\theta}\right)^{k-1} E_x.$$

The bridge scaling factor is

$$\beta(\psi) = \frac{F_1(b) - F_1(a)}{F_2(b) - F_2(a)} = \frac{R_a - R_b}{E_a - E_b}.$$

Accordingly, the EWE distribution and CDF and pdf in equation 3 and 4 respectively. The eight estimation methods used in the simulation study are developed below. All estimators are obtained by optimizing their corresponding criterion over the admissible parameter space.

© 2026 NSP
Natural Sciences Publishing Cor.

4.1 Derivatives Required for the Estimating Equations

Because the same derivatives of the EWE CDF occur in several estimation methods, they are derived once here and then used throughout the section. Write

$$A = R_a - R_b, \qquad B = E_a - E_b, \qquad \beta = \frac{A}{B}.$$

The nonzero derivatives of A are

$$A_\lambda = -aR_a + bR_b, \qquad A_a = -\lambda R_a, \qquad A_b = \lambda R_b.$$

The derivatives of B are

$$B_k = -E_a z_a log\left(\frac{a}{\theta}\right) + E_b z_b log\left(\frac{b}{\theta}\right),$$

$$B_\theta = \frac{k}{\theta}\left(E_a z_a - E_b z_b\right),$$

$$B_a = -\frac{k}{a}E_a z_a, \qquad B_b = \frac{k}{b}E_b z_b.$$

Therefore, for any component ψ_j of ψ,

$$\beta_j \equiv \frac{\partial \beta}{\partial \psi_j} = \frac{A_j B - A B_j}{B^2},$$

with $A_k = A_\theta = B_\lambda = 0$. Equivalently,

$$\frac{\partial log\beta}{\partial \psi_j} = \frac{A_j}{A} - \frac{B_j}{B}.$$

For x in either exponential region, $x < a$ or $x > b$,

$$\frac{\partial F(x;\psi)}{\partial \lambda} = xe^{-\lambda x}, \qquad \frac{\partial F(x;\psi)}{\partial k} = \frac{\partial F(x;\psi)}{\partial \theta} = \frac{\partial F(x;\psi)}{\partial a} = \frac{\partial F(x;\psi)}{\partial b} = 0,$$

provided that x is not crossing a breakpoint during the local differentiation. For the bridge region $a < x < b$, define

$$C_x = F_2(x) - F_2(b) = E_b - E_x.$$

Its required derivatives are

$$(C_x)_k = -E_b z_b log\left(\frac{b}{\theta}\right) + E_x z_x log\left(\frac{x}{\theta}\right),$$

$$(C_x)_\theta = \frac{k}{\theta}\left(E_b z_b - E_x z_x\right), \qquad (C_x)_a = 0, \qquad (C_x)_b = -\frac{k}{b}E_b z_b.$$

Hence, in the bridge region,

$$F_\lambda(x) = be^{-\lambda b} + \beta_\lambda C_x,$$

$$F_k(x) = \beta_k C_x + \beta\left(C_x\right)_k,$$

$$F_\theta(x) = \beta_\theta C_x + \beta\left(C_x\right)_\theta,$$

$$F_a(x) = \beta_a C_x,$$

and

© 2026 NSP
Natural Sciences Publishing Cor.

$$F_b(x) = \lambda e^{-\lambda b} + \beta_b C_x - \beta \frac{k}{b} E_b z_b.$$

These derivatives are valid on regions where the membership of each observation relative to a and b is unchanged. Since changing a breakpoint can move observations from one piece of the density to another, the global objective is generally non-smooth in a and b. This is why derivative-free numerical optimization is appropriate for the complete five-parameter problem.

4.2 Maximum Likelihood Estimation (MLE)

Let $\mathscr{I}_O = \{i : X_i < a \text{ or } X_i > b\}$, $\mathscr{I}_M = \{i : a < X_i < b\}$, and let $n_O = |\mathscr{I}_O|$, $n_M = |\mathscr{I}_M|$. The likelihood function is

$$L(\psi) = \prod_{i \in \mathscr{I}_O} \lambda e^{-\lambda X_i} \prod_{i \in \mathscr{I}_M} \left[\beta \frac{k}{\theta} \left(\frac{X_i}{\theta} \right)^{k-1} e^{-(X_i/\theta)^k} \right]. \tag{15}$$

Taking logarithms gives

$$\updownarrow(\psi) = n_O log\lambda - \lambda \sum_{i \in \mathscr{I}_O} X_i + n_M log\beta + n_M logk - n_M klog\theta + (k-1) \sum_{i \in \mathscr{I}_M} \log X_i - \sum_{i \in \mathscr{I}_M} \left(\frac{X_i}{\theta} \right)^k. \tag{16}$$

For fixed membership sets $\mathscr{I}_O$ and $\mathscr{I}_M$, the score equations are

$$U_\lambda = \frac{n_O}{\lambda} - \sum_{i \in \mathscr{I}_O} X_i + n_M \frac{\partial log\beta}{\partial \lambda} = 0,$$

$$U_k = \frac{n_M}{k} + \sum_{i \in \mathscr{I}_M} \left[1 - \left(\frac{X_i}{\theta} \right)^k \right] log \left(\frac{X_i}{\theta} \right) + n_M \frac{\partial log\beta}{\partial k} = 0,$$

$$U_\theta = \frac{k}{\theta} \sum_{i \in \mathscr{I}_M} \left[\left(\frac{X_i}{\theta} \right)^k - 1 \right] + n_M \frac{\partial log\beta}{\partial \theta} = 0,$$

$$U_a = n_M \frac{\partial log\beta}{\partial a} = 0, \qquad U_b = n_M \frac{\partial log\beta}{\partial b} = 0.$$

Because the data classification changes when a or b passes an observation, the likelihood is not globally differentiable in the breakpoints. Thus, the MLE is computed numerically as

$$\widehat{\psi}_{MLE} = arg \min_{\psi \in \Omega} \{ -\updownarrow(\psi) \}. \tag{17}$$

This is exactly the negative-log-likelihood criterion used in the simulation.

4.3 Least Squares Estimation (LSE)

Let $X_{(1)} \leq \cdots \leq X_{(n)}$ denote the ordered sample. Under the probability-integral transformation, $F\left(X_{(i)}; \psi\right)$ behaves like the i-th order statistic from a standard uniform distribution, whose mean is

$$E\left[U_{(i)}\right] = \frac{i}{n+1}.$$

The LSE criterion therefore minimizes the squared discrepancy between the fitted CDF and these expected uniform order statistics:

$$S_{LSE}(\psi) = \sum_{i=1}^{n} \left[F\left(X_{(i)}; \psi\right) - \frac{i}{n+1} \right]^2.$$

Hence,

© 2026 NSP
Natural Sciences Publishing Cor.

$$\widehat{\psi}_{LSE} = arg \min_{\psi \in \Omega} S_{LSE}(\psi).$$

Differentiating with respect to ψ_j yields

$$\frac{\partial S_{LSE}}{\partial \psi_j} = 2\sum_{i=1}^{n} \left[F_i - \frac{i}{n+1} \right] F_{ij}, \tag{18}$$

where

$$F_i = F\left(X_{(i)}; \psi\right), \qquad F_{ij} = \frac{\partial F\left(X_{(i)}; \psi\right)}{\partial \psi_j}.$$

Thus, the five LSE estimating equations are

$$\sum_{i=1}^{n} \left[F_i - \frac{i}{n+1} \right] F_{ij} = 0, \qquad j = 1, \ldots, 5. \tag{19}$$

The derivatives F_{ij} are the piecewise quantities derived in section 4.

4.4 Weighted Least Squares Estimation (WLSE)

For a standard uniform order statistic,

$$Var\left(U_{(i)}\right) = \frac{i(n-i+1)}{(n+1)^2(n+2)}.$$

Consequently, the inverse-variance weight used in the simulation is

$$w_i = \frac{(n+1)^2(n+2)}{i(n-i+1)}.$$

The WLSE objective function is

$$S_{WLSE}(\psi) = \sum_{i=1}^{n} w_i \left[F\left(X_{(i)}; \psi\right) - \frac{i}{n+1} \right]^2.$$

Therefore,

$$\widehat{\psi}_{WLSE} = arg \min_{\psi \in \Omega} S_{WLSE}(\psi),$$

and the corresponding estimating equations are

$$\frac{\partial S_{WLSE}}{\partial \psi_j} = 2\sum_{i=1}^{n} w_i \left[F_i - \frac{i}{n+1} \right] F_{ij} = 0, \qquad j = 1, \ldots, 5. \tag{20}$$

Thus, WLSE has the same estimating structure as LSE but assigns greater importance to order statistics whose transformed sampling variance is smaller.

4.5 Cramer-von Mises Estimation (CVM)

The Cramer-von Mises criterion measures the integrated squared discrepancy between the fitted CDF and the empirical distribution function. In order-statistic form, the criterion used in the simulation is

$$S_{CVM}(\psi) = \frac{1}{12n} + \sum_{i=1}^{n} \left[F\left(X_{(i)}; \psi\right) - \frac{2i-1}{2n} \right]^2.$$

The CVM estimator is

© 2026 NSP
Natural Sciences Publishing Cor.

$$\widehat{\psi}_{CVM} = arg \min_{\psi \in \Omega} S_{CVM}(\psi).$$

Since $1/(12n)$ is constant with respect to the parameters,

$$\frac{\partial S_{CVM}}{\partial \psi_j} = 2\sum_{i=1}^{n}\left[F_i - \frac{2i-1}{2n}\right]F_{ij}.$$

Accordingly, the CVM estimating equations are

$$\sum_{i=1}^{n}\left[F_i - \frac{2i-1}{2n}\right]F_{ij} = 0, \qquad j = 1,\ldots,5. \tag{21}$$

4.6 Anderson-Darling Estimation (AD)

The Anderson-Darling criterion places relatively greater emphasis on discrepancies in the tails. Define

$$F_i = F\left(X_{(i)};\psi\right), \qquad F_{n+1-i} = F\left(X_{(n+1-i)};\psi\right).$$

The objective function used in the simulation is

$$S_{AD}(\psi) = -n - \frac{1}{n}\sum_{i=1}^{n}(2i-1)\left[\log F_i + log\left(1-F_{n+1-i}\right)\right].$$

Hence,

$$\widehat{\psi}_{AD} = arg \min_{\psi \in \Omega} S_{AD}(\psi).$$

Differentiation gives

$$\frac{\partial S_{AD}}{\partial \psi_j} = -\frac{1}{n}\sum_{i=1}^{n}(2i-1)\left[\frac{F_{ij}}{F_i} - \frac{F_{n+1-i,j}}{1-F_{n+1-i}}\right],$$

so that the AD estimating equations are

$$\sum_{i=1}^{n}(2i-1)\left[\frac{F_{ij}}{F_i} - \frac{F_{n+1-i,j}}{1-F_{n+1-i}}\right] = 0, \qquad j = 1,\ldots,5. \tag{22}$$

For numerical stability, fitted CDF values extremely close to zero or one are bounded away from the endpoints before the logarithms are evaluated.

4.7 Maximum Product Spacings Estimation (MPS)

Let $U_i = F\left(X_{(i)};\psi\right), \qquad i = 1,\ldots,n$, and define $U_0 = 0$ and $U_{n+1} = 1$. The probability spacings are

$$D_i(\psi) = U_i - U_{i-1}, \qquad i = 1,\ldots,n+1.$$

Thus,

$$D_1 = F\left(X_{(1)};\psi\right), \quad D_i = F\left(X_{(i)};\psi\right) - F\left(X_{(i-1)};\psi\right), \qquad i = 2,\ldots,n,$$

and

$$D_{n+1} = 1 - F\left(X_{(n)};\psi\right).$$

The maximum product spacings estimator maximizes

$$G(\psi) = \prod_{i=1}^{n+1} D_i(\psi),$$

© 2026 NSP
Natural Sciences Publishing Cor.

or, equivalently, minimizes

$$S_{MPS}(\psi) = -\sum_{i=1}^{n+1} \log D_i(\psi). \tag{23}$$

Therefore,

$$\widehat{\psi}_{MPS} = arg\min_{\psi\in\Omega} S_{MPS}(\psi).$$

The derivatives of the spacings are

$$D_{1,j} = F_{1j}, \quad D_{i,j} = F_{ij} - F_{i-1,j}, \qquad i = 2,\ldots,n,$$

and

$$D_{n+1,j} = -F_{nj}.$$

Hence,

$$\frac{\partial S_{MPS}}{\partial \psi_j} = -\sum_{i=1}^{n+1} \frac{D_{i,j}}{D_i},$$

and the five MPS estimating equations are

$$\sum_{i=1}^{n+1} \frac{D_{i,j}}{D_i} = 0, \qquad j = 1,\ldots,5. \tag{24}$$

In computation, extremely small spacings are replaced by a positive machine-level tolerance before taking logarithms.

4.8 Percentile Matching Estimation (PM)

Let $Q(p;\psi) = F^{-1}(p;\psi)$ denote the EWE quantile function. Define

$$F_a = 1 - e^{-\lambda a}, \qquad F_b = 1 - e^{-\lambda b}.$$

Then

$$Q(p;\psi) = \begin{cases} -\frac{\log(1-p)}{\lambda}, & 0 < p \le F_a, \\ \theta\left[-log\,(1-v_p)\right]^{1/k}, & F_a < p \le F_b, \\ -\frac{\log(1-p)}{\lambda}, & F_b < p < 1, \end{cases} \tag{25}$$

where

$$v_p = F_2(b) + \frac{p - F_b}{\beta}.$$

Because the EWE model contains five unknown parameters, the percentile-matching procedure used in the simulation employs five probabilities,

$$\mathscr{P}_{PM} = \{0.10,\ 0.25,\ 0.50,\ 0.75,\ 0.90\}.$$

Let $q_s(p)$ denote the corresponding sample percentile and $Q(p;\psi)$ the model percentile. The PM criterion is

$$S_{PM}(\psi) = \sum_{p\in\mathscr{P}_{PM}} \left[Q(p;\psi) - q_s(p)\right]^2.$$

Thus,

$$\widehat{\psi}_{PM} = arg\min_{\psi\in\Omega} S_{PM}(\psi).$$

© 2026 NSP
Natural Sciences Publishing Cor.

For a probability p lying away from a breakpoint probability, the implicit identity

$$F\left(Q(p;\psi);\psi\right)=p$$

gives

$$\frac{\partial Q(p;\psi)}{\partial \psi_j}=-\frac{F_j\left(Q(p;\psi);\psi\right)}{f\left(Q(p;\psi);\psi\right)}.$$

Consequently,

$$\frac{\partial S_{PM}}{\partial \psi_j}=2\sum_{p\in\mathscr{P}_{PM}}\left[Q(p;\psi)-q_s(p)\right]Q_j(p;\psi),$$

and the five PM estimating equations are

$$\sum_{p\in\mathscr{P}_{PM}}\left[Q(p;\psi)-q_s(p)\right]Q_j(p;\psi)=0,\qquad j=1,\ldots,5. \tag{26}$$

In the simulation implementation, the sample percentiles were computed using the R type-8 quantile definition.

4.9 Quantile Least Squares Estimation (QLS)

Quantile least squares extends percentile matching by fitting the model to a denser grid of empirical quantiles. The probability grid used in the simulation is

$$\mathscr{P}_{QLS}=\{0.10,0.20,0.30,0.40,0.50,0.60,0.70,0.80,0.90\}.$$

The objective function is

$$S_{QLS}(\psi)=\sum_{p\in\mathscr{P}_{QLS}}\left[Q(p;\psi)-q_s(p)\right]^2.$$

Hence,

$$\widehat{\psi}_{QLS}=arg\min_{\psi\in\Omega}S_{QLS}(\psi).$$

Using the quantile derivative in (26),

$$\frac{\partial S_{QLS}}{\partial \psi_j}=2\sum_{p\in\mathscr{P}_{QLS}}\left[Q(p;\psi)-q_s(p)\right]Q_j(p;\psi),$$

so the QLS estimating equations are

$$\sum_{p\in\mathscr{P}_{QLS}}\left[Q(p;\psi)-q_s(p)\right]Q_j(p;\psi)=0,\qquad j=1,\ldots,5. \tag{27}$$

The essential difference between PM and QLS in this study is therefore the number of quantiles fitted: PM uses five selected percentiles, while QLS uses nine quantiles spanning the central 10% to 90% range.

4.10 Numerical Optimization and Parameter Constraints

The eight criteria above generally do not lead to closed-form solutions for all five EWE parameters. Moreover, the free breakpoints make the objective functions potentially non-smooth. For this reason, the simulation used direct numerical minimization. To enforce$\lambda>0,k>0,\theta>0,a>0,b>a$,the unconstrained working vector $z=(z_1,z_2,z_3,z_4,z_5)^{\mathsf{T}}$ was mapped to the original parameter space through

$$\lambda=e^{z_1},\qquad k=e^{z_2},\qquad \theta=e^{z_3},\qquad a=e^{z_4},\qquad b=a+e^{z_5}. \tag{28}$$

© 2026 NSP
Natural Sciences Publishing Cor.

Equivalently, the starting parameter vector is encoded as

$$z_1 = log\lambda, \qquad z_2 = logk, \qquad z_3 = log\theta, \qquad z_4 = loga, \qquad z_5 = log(b-a). \tag{29}$$

Each objective function was minimized with the Nelder-Mead algorithm using the transformed parameters. This ensures accurate estimates at every numerical iteration and does not force us to create an inequality. The same optimization framework was applied for MLE, LSE, WLSE, CVM, AD, MPS, PM, and QLS, ensuring that the simulation comparison reflects differences among the statistical criteria rather than differences in the optimization mechanism.

4.11 Summary of the Eight Estimators

The resulting estimators can be written compactly as

$$\widehat{\psi}_m = arg\min_{\psi\in\Omega} S_m(\psi), \qquad m \in \{MLE, LSE, WLSE, CVM, AD, MPS, PM, QLS\}, \tag{30}$$

Here S_MLE(ψ) = -$\ell(\psi)$, and each of the other seven criteria is defined in Subsections 4.3–4.9. The eight estimators target the five EWE parameters (λ, k, θ, a, b).

5 Simulation Design

We performed a Monte Carlo experiment to test the finite sample behaviour of eight estimators for the five parameters of the Exponential-Weibull-Exponential (EWE) Spliced-Bridge distribution. The true parameter vector was fixed to $(\lambda, k, \theta, a, b) = (0.5,\ 2,\ 3,\ 2,\ 6)$. Four sample sizes were considered (n = 20, 50, 125, 250) and each case was repeated 1,000 times. The estimation methods used were maximum likelihood (MLE), least squares (LSE), weighted least squares (WLSE), Cramér-von Mises (CVM), Anderson-Darling (AD), maximum product spacings (MPS), percentile matching (PM), quantile least squares (QLS). We evaluated the performance with the Monte Carlo mean, absolute bias, mean squared error (MSE), root mean squared error (RMSE), standard deviation, mean absolute error (MAE), convergence rate and a composite rank.

Table 2: Monte Carlo simulation design.

Simulation component	Setting
True parameters	$\lambda = 0.5,\ k = 2,\ \theta = 3,\ a = 2,\ b = 6$
Sample sizes	$n = 20,\ 50,\ 125,\ 250$
Replications	1,000 per sample size
Estimation methods	MLE, LSE, WLSE, CVM, AD, MPS, PM, QLS
Primary criteria	Mean, Bias, MSE, RMSE, SD, MAE, convergence, rank

The following tables present the Monte Carlo analysis for all four sample sizes, all five EWE parameters and all eight estimation methods. No sample size is omitted in the numerical analysis. The highlighted cell in each row shows the best method for each parameter and sample size if the criterion holds.

For a statistically non-redundant overall comparison, the rank was re-calculated from the actual Bias, MSE, MAE, and SD values. For each parameter, the lowest criterion value gives the best rank. The ranks are then averaged over all five parameters and over the four criteria. RMSE is not used again in the composite score as it is a monotone transformation of MSE and would duplicate the same ordering. Lower composite scores indicate better overall performance.

The simulation clearly demonstrates the transition from small-sample robustness to large-sample efficiency. PM provides the best composite performance at n = 20, followed by MLE, QLS, and MPS. This is because the percentile information is stable when the sample is small and the likelihood surface is not very tough, especially since the EWE model has two free breakpoints. At n = 50 PM remains the best composite estimator but the difference between PM and MLE is much smaller. By n = 125 and n = 250, MLE becomes the most efficient estimator and we can see that the likelihood-based efficiency increases as the sample is richer in terms of information about the continuous parameters and the change points.

© 2026 NSP
Natural Sciences Publishing Cor.

Table 3: Monte Carlo Mean Estimates. Green cells indicate the best value within each sample-size/parameter combination.

n	Para.	MLE	LSE	WLSE	CVM	AD	MPS	PM	QLS
	λ	0.530447	0.584293	0.580699	0.553048	0.551540	**0.504568**	0.528737	0.528084
	k	2.91995	2.47838	2.32912	2.57242	2.52112	3.62626	**2.18187**	2.37001
20	θ	3.95172	4.55466	4.57694	4.12593	4.19892	4.37880	**3.45656**	4.10562
	a	2.09837	1.69919	1.71938	1.76529	1.77501	2.10922	**1.97814**	1.92479
	b	8.22493	8.76504	9.01772	9.12496	9.21877	**7.20311**	7.21912	8.45033
	λ	**0.506485**	0.541507	0.540542	0.528789	0.526333	0.489840	0.517182	0.519365
	k	2.48499	2.24891	2.09983	2.22648	**2.06434**	2.62428	2.07141	2.31012
50	θ	3.57534	3.83919	3.75420	3.67938	3.74145	3.90297	**3.33279**	3.85969
	a	2.07407	1.74796	1.75664	1.79862	1.80161	2.10643	1.99410	**2.00092**
	b	6.99134	9.03672	9.35840	9.14713	9.59238	6.96509	**6.93605**	8.22569
	λ	**0.501784**	0.515734	0.512378	0.511052	0.509791	0.491980	0.509892	0.510057
	k	2.33670	2.07604	1.96180	2.09962	**1.99860**	2.35277	2.02599	2.31413
125	θ	3.23175	3.31078	**3.07022**	3.23521	3.12167	3.25641	3.18704	3.35119
	a	2.04265	1.76661	1.79542	1.77264	1.81126	2.05933	**2.01509**	2.05413
	b	**6.34883**	8.51620	9.04340	8.80902	9.20888	6.41897	6.57799	8.06184
	λ	**0.500169**	0.507833	0.507028	0.506158	0.505740	0.495115	0.504639	0.505927
	k	2.23903	2.05768	1.94743	2.04515	1.92539	2.28800	**2.01024**	2.17173
250	θ	3.14378	3.16046	3.04610	3.08671	**2.96596**	3.14729	3.12915	3.19082
	a	**2.05004**	1.81544	1.80841	1.78593	1.79132	2.05331	2.05596	2.09463
	b	**6.17895**	8.47992	8.87824	8.35389	8.98920	6.20481	6.45921	8.06813

Table 4: Absolute Bias. Green cells indicate the best value within each sample-size/parameter combination.

n	Para.	MLE	LSE	WLSE	CVM	AD	MPS	PM	QLS
	λ	0.030447	0.084293	0.080699	0.053048	0.051540	**0.004568**	0.028737	0.028084
	k	0.919948	0.478380	0.329122	0.572417	0.521117	1.62626	**0.181873**	0.370010
20	θ	0.951721	1.55466	1.57694	1.12593	1.19892	1.37880	**0.456563**	1.10562
	a	0.098374	0.300809	0.280617	0.234714	0.224993	0.109215	**0.021860**	0.075212
	b	2.22493	2.76504	3.01772	3.12496	3.21877	**1.20311**	1.21912	2.45033
	λ	**0.006485**	0.041507	0.040542	0.028789	0.026333	0.010160	0.017182	0.019365
	k	0.484989	0.248914	0.099831	0.226479	**0.064337**	0.624281	0.071405	0.310117
50	θ	0.575335	0.839192	0.754203	0.679378	0.741453	0.902967	**0.332785**	0.859686
	a	0.074073	0.252041	0.243364	0.201384	0.198390	0.106435	0.005904	**0.000917**
	b	0.991344	3.03672	3.35840	3.14713	3.59238	0.965095	**0.936052**	2.22569
	λ	**0.001784**	0.015734	0.012378	0.011052	0.009791	0.008020	0.009892	0.010057
	k	0.336695	0.076039	0.038201	0.099615	**0.001403**	0.352772	0.025986	0.314130
125	θ	0.231747	0.310777	**0.070222**	0.235207	0.121670	0.256409	0.187044	0.351195
	a	0.042651	0.233391	0.204581	0.227359	0.188742	0.059331	**0.015087**	0.054125
	b	**0.348826**	2.51620	3.04340	2.80902	3.20888	0.418966	0.577994	2.06184
	λ	**0.000169**	0.007833	0.007028	0.006158	0.005740	0.004885	0.004639	0.005927
	k	0.239029	0.057676	0.052573	0.045154	0.074613	0.287997	**0.010236**	0.171734
250	θ	0.143783	0.160458	0.046103	0.086709	**0.034038**	0.147292	0.129154	0.190816
	a	**0.050042**	0.184556	0.191592	0.214071	0.208682	0.053309	0.055964	0.094635
	b	**0.178955**	2.47992	2.87824	2.35389	2.98920	0.204811	0.459210	2.06813

The parameter-specific results show that λ is the easiest parameter to estimate accurately. For λ, MPS gives the smallest MSE and RMSE at every investigated sample size while MLE has very small bias as n increases. For n = 250, the MLE mean for λ is 0.500169 and the absolute bias is only 0.000169, but MPS has a slightly smaller MSE (0.001115) than MLE (0.001183). This is a good example of the bias-variance trade-off. The estimator with the smallest bias is not

© 2026 NSP
Natural Sciences Publishing Cor.

Table 5: Mean Squared Error (MSE). Green cells indicate the best value within each sample-size/parameter combination.

n	Para.	MLE	LSE	WLSE	CVM	AD	MPS	PM	QLS
	λ	0.027419	0.076839	0.084433	0.059171	0.058721	**0.023551**	0.040710	0.040054
	k	3.70149	4.81908	4.37287	5.01202	4.67360	8.81995	**1.22847**	3.14541
20	θ	8.80119	20.99976	21.58907	18.11468	18.87736	16.85021	**4.36265**	12.16989
	a	**0.233212**	0.786997	0.879730	0.759036	0.917842	0.341943	0.513854	0.723582
	b	20.92622	27.96231	29.46124	30.92092	30.85815	14.31877	**7.74117**	21.90380
	λ	0.007888	0.026348	0.031407	0.021647	0.024268	**0.007049**	0.014101	0.014273
	k	1.37665	3.93772	3.35043	3.61160	3.06931	2.76729	**0.959821**	2.49273
50	θ	3.67737	12.76007	12.26387	11.73269	13.22575	10.23661	**1.66409**	8.50746
	a	**0.144998**	0.812453	0.951734	0.809935	0.889864	0.219874	0.473241	0.626057
	b	6.21382	29.21693	30.91895	30.72444	33.15159	8.11839	**5.29760**	20.36625
	λ	0.002691	0.008802	0.009305	0.008380	0.009469	**0.002498**	0.005244	0.005065
	k	**0.481414**	2.55771	2.35794	2.52995	2.42695	0.919311	0.504628	1.95896
125	θ	**0.477061**	7.86470	6.08435	7.34068	7.00034	1.94310	0.788025	2.94455
	a	**0.064318**	0.683340	0.836038	0.722883	0.837127	0.097207	0.331593	0.518997
	b	**0.651526**	24.05924	28.06735	26.07670	29.66208	1.35733	3.08639	19.79752
	λ	0.001183	0.003272	0.004138	0.003255	0.003891	**0.001115**	0.002009	0.001944
	k	**0.249078**	2.03311	1.85491	1.95737	1.75655	0.432755	0.273158	1.07215
250	θ	**0.124034**	5.37634	5.23429	4.61617	4.29407	0.357223	0.362511	1.37191
	a	**0.037515**	0.674864	0.811623	0.707023	0.805230	0.051995	0.222265	0.437817
	b	**0.201050**	24.17811	26.95381	21.90289	27.46601	0.359594	2.16028	20.03716

Table 6: Root Mean Squared Error (RMSE). Green cells indicate the best value within each sample-size/parameter combination.

n	Para.	MLE	LSE	WLSE	CVM	AD	MPS	PM	QLS
	λ	0.165585	0.277199	0.290574	0.243251	0.242323	**0.153464**	0.201768	0.200135
	k	1.92392	2.19524	2.09114	2.23875	2.16185	2.96984	**1.10836**	1.77353
20	θ	2.96668	4.58255	4.64640	4.25613	4.34481	4.10490	**2.08869**	3.48854
	a	**0.482921**	0.887128	0.937939	0.871227	0.958040	0.584759	0.716836	0.850636
	b	4.57452	5.28794	5.42782	5.56066	5.55501	3.78402	**2.78230**	4.68015
	λ	0.088816	0.162320	0.177219	0.147129	0.155782	**0.083956**	0.118746	0.119468
	k	1.17331	1.98437	1.83042	1.90042	1.75194	1.66352	**0.979705**	1.57884
50	θ	1.91765	3.57212	3.50198	3.42530	3.63672	3.19947	**1.29000**	2.91676
	a	**0.380786**	0.901362	0.975569	0.899964	0.943326	0.468907	0.687925	0.791237
	b	2.49275	5.40527	5.56048	5.54296	5.75774	2.84928	**2.30165**	4.51290
	λ	0.051878	0.093817	0.096462	0.091540	0.097309	**0.049978**	0.072415	0.071169
	k	**0.693840**	1.59928	1.53556	1.59058	1.55787	0.958807	0.710371	1.39963
125	θ	**0.690696**	2.80441	2.46665	2.70937	2.64582	1.39395	0.887708	1.71597
	a	**0.253611**	0.826644	0.914351	0.850225	0.914946	0.311781	0.575841	0.720414
	b	**0.807172**	4.90502	5.29786	5.10653	5.44629	1.16504	1.75681	4.44944
	λ	0.034402	0.057201	0.064326	0.057057	0.062376	**0.033393**	0.044817	0.044094
	k	**0.499077**	1.42587	1.36195	1.39906	1.32535	0.657841	0.522645	1.03545
250	θ	**0.352184**	2.31869	2.28786	2.14853	2.07221	0.597681	0.602089	1.17129
	a	**0.193688**	0.821501	0.900901	0.840847	0.897346	0.228025	0.471450	0.661677
	b	**0.448386**	4.91712	5.19171	4.68005	5.24080	0.599661	1.46979	4.47629

required to have the smallest MSE. For k and θ, PM looks particularly attractive at the smallest samples. At n = 20, PM gives the smallest bias and the smallest MSE/RMSE for both parameters. But the relative advantage changes with increasing n. At n = 125, MLE has the smallest MSE for k and θ and at n = 250 its MSE values decrease to 0.2491 and

© 2026 NSP
Natural Sciences Publishing Cor.

Table 7: Percentage of successful numerical fits over the 1,000 replications.

n	MLE	LSE	WLSE	CVM	AD	MPS	PM	QLS
20	99.8%	100.0%	100.0%	100.0%	99.9%	99.9%	99.9%	99.2%
50	99.3%	100.0%	99.9%	99.9%	99.8%	100.0%	99.8%	99.8%
125	99.3%	100.0%	99.9%	100.0%	100.0%	99.8%	100.0%	99.9%
250	99.4%	99.9%	99.6%	99.5%	99.8%	99.7%	100.0%	100.0%

Table 8: Composite ranks by sample size; green rows identify the best method.

n	Method	Bias rank	MSE rank	MAE rank	SD rank	Composite score	Overall rank
20	**PM**	**1.60**	**2.00**	**2.00**	**2.00**	**1.900**	**1**
	MLE	3.80	2.20	2.20	2.20	2.600	2
	QLS	2.80	3.20	3.20	3.60	3.200	3
	MPS	4.00	3.40	3.40	3.40	3.550	4
	AD	5.60	6.20	6.20	6.20	6.050	5
	CVM	5.80	6.20	6.20	6.20	6.100	6
	LSE	6.40	6.20	6.20	5.80	6.150	7
	WLSE	6.00	6.60	6.60	6.60	6.450	8
50	**PM**	**1.80**	**1.80**	**2.00**	**1.80**	**1.850**	**1**
	MLE	3.20	1.80	1.80	1.80	2.150	2
	MPS	4.80	2.80	2.80	2.60	3.250	3
	QLS	4.40	3.60	3.40	3.80	3.800	4
	CVM	5.00	5.60	5.60	6.20	5.600	5
	AD	4.60	6.80	6.80	6.60	6.200	6
	LSE	6.40	6.60	6.60	6.60	6.550	7
	WLSE	5.80	7.00	7.00	6.60	6.600	8
125	**MLE**	**3.00**	**1.20**	**1.20**	**1.20**	**1.650**	**1**
	MPS	4.40	2.20	2.20	2.20	2.750	2
	PM	2.60	2.80	2.80	2.80	2.750	3
	QLS	5.20	3.80	3.80	3.80	4.150	4
	WLSE	4.80	6.20	7.00	6.20	6.050	5
	CVM	5.80	6.20	6.00	6.20	6.050	6
	AD	3.80	7.20	6.80	7.20	6.250	7
	LSE	6.40	6.40	6.20	6.40	6.350	8
250	**MLE**	**3.00**	**1.20**	**1.20**	**1.20**	**1.650**	**1**
	MPS	4.20	2.00	2.20	2.00	2.600	2
	PM	2.60	3.00	2.80	3.00	2.850	3
	QLS	5.40	3.80	3.80	3.80	4.200	4
	CVM	4.80	5.80	5.80	6.00	5.600	5
	AD	5.00	6.40	6.60	6.20	6.050	6
	LSE	6.00	6.60	6.20	6.40	6.300	7
	WLSE	5.00	7.20	7.40	7.40	6.750	8

0.1240. So while a number of methods can produce means close to the true values, MLE becomes much less dispersed and therefore does much better quadratic-loss performance in large samples.

The breakpoint parameters a and b are more difficult than λ. For a, MLE has the smallest MSE at every sample size shown, even if PM or QLS have a smaller absolute bias. This shows that bias alone is not enough for judging the quality of estimators. For b, again the small-sample problem is more pronounced: at n = 20 the mean of MLE is 8.2249 while the true one is 6 and RMSE is 4.5745. PM improves RMSE to 2.7823 in that case. However, when n increases, the MLE estimate starts to stabilize and with n = 250, the mean is 6.1790 and RMSE is 0.4484, which is the smallest among all methods for b.

© 2026 NSP
Natural Sciences Publishing Cor.

Table 9: Final composite ranking over n = 20, 50, 125, and 250.

Final rank	Method	Average composite score
1	**MLE**	**2.013**
2	**PM**	2.337
3	**MPS**	3.038
4	**QLS**	3.838
5	**CVM**	5.837
6	**AD**	6.137
7	**LSE**	6.338
8	**WLSE**	6.462

The MLE mean squared error falls from n = 20 to n = 250 by approximately 95.7% for λ, 93.3% for k, 98.6% for θ, 83.9% for a, and 99.0% for b. This is evidence of improved finite-sample accuracy under the investigated parameter configuration, rather than a formal proof of estimator consistency. In contrast, estimation of the upper breakpoint b remains difficult for some CDF-based criteria: at n = 250, the MSE values are 24.18 for LSE, 26.95 for WLSE, 21.90 for CVM, and 27.47 for AD, compared with 0.201 for MLE and 0.360 for MPS. Across all settings, the successful-fit rates range from 99.2% to 100.0%, showing that numerical termination alone cannot account for the large differences in estimation error. The final composite ranking is MLE, PM, MPS, QLS, CVM, AD, LSE and WLSE (Table 9). PM is competitive in small samples, whereas MLE is preferred at moderate and large sample sizes in the present study. Figures 4 and 5 and the accompanying R graphics show the corresponding sampling dispersion, bias, and running-mean behaviour using the actual 1,000-replication output; Tables 3—9 retain every original numerical result.

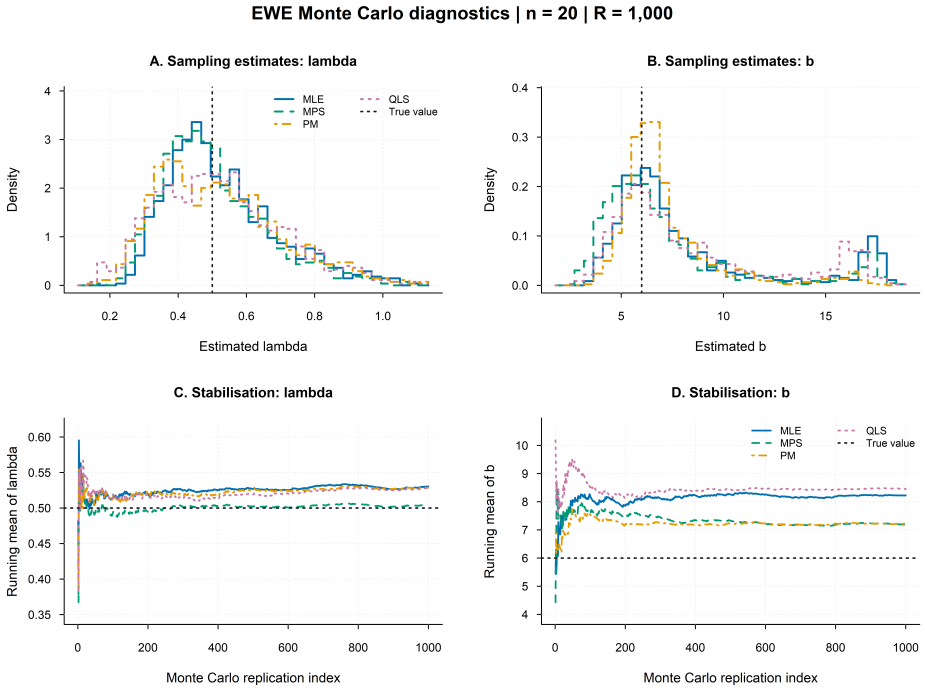

Fig. 4: Monte Carlo diagnostics for n = 20 (1,000 original replications; R-generated graphics). (A) Sampling densities of the exponential rate λ; (B) sampling densities of the upper breakpoint b; (C) cumulative running means of λ; (D) cumulative running means of b. MLE, MPS, PM and QLS are distinguished by colour and line type; black dotted lines mark the generating values $\lambda = 0.5$ and b = 6.

© 2026 NSP
Natural Sciences Publishing Cor.

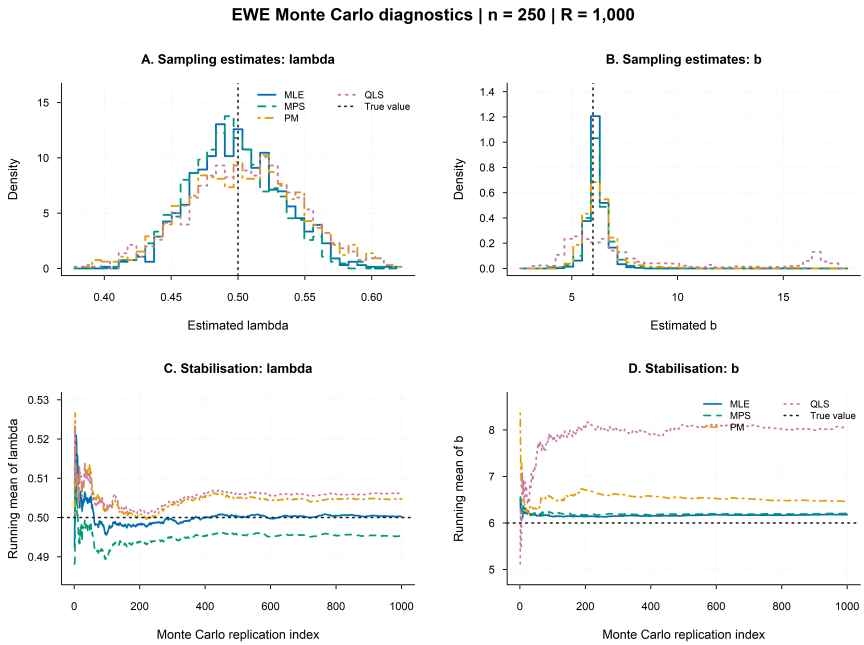

Fig. 5: Monte Carlo diagnostics for n = 250 (1,000 original replications; R-generated graphics). Panels (A)–(D), estimator colors, line types and reference values follow Figure 4. The running means are calculated across Monte Carlo replications, not across numerical optimization iterations.

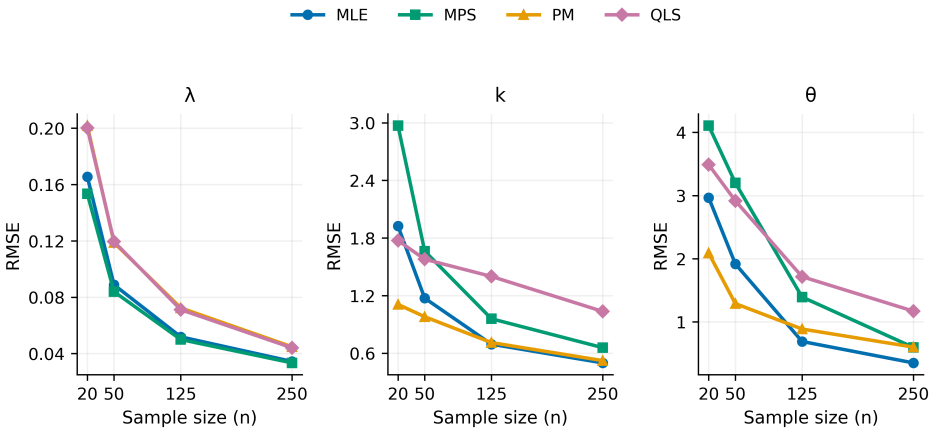

Fig. 6: RMSE by sample size for the exponential rate λ, Weibull shape k, and Weibull scale θ. The four leading methods are shown; the full eight-method comparison is retained in Table 6.

© 2026 NSP
Natural Sciences Publishing Cor.

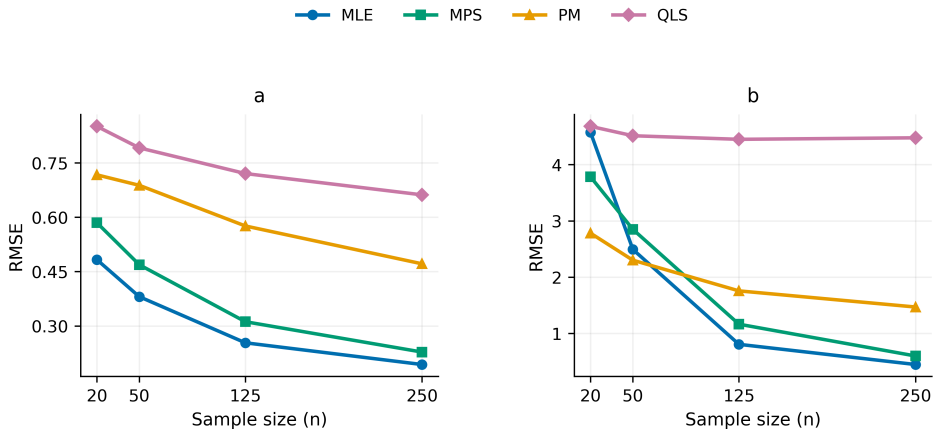

Fig. 7: RMSE by sample size for the lower breakpoint a and upper breakpoint b. Curves use the original Table 6 values and distinguish methods through line colour and markers.

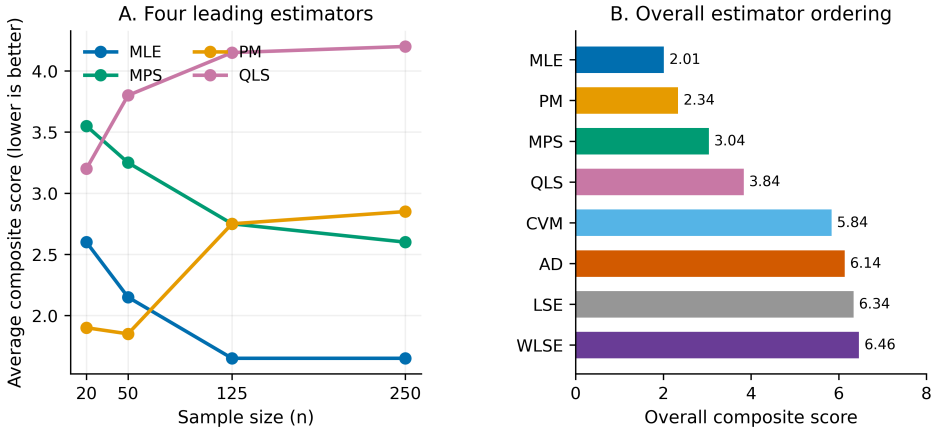

Fig. 8: Composite estimator ranking. (A) Average score across the four sample sizes for the four leading estimators; (B) average composite score across sample sizes for all eight methods, from Tables 8 and 9. Lower is better.

Figures 4 and 5 display the original R-produced Monte Carlo diagnostics for n = 20 and n = 250, respectively. Panels A and B show the replicate-level sampling distributions of λ and b for MLE, MPS, PM and QLS, while panels C and D trace cumulative means across the 1,000 replications. At n = 20, the estimated upper breakpoint b has a pronounced right tail and the running means remain substantially above the generating value of 6. At n = 250, the MLE estimates concentrate much closer to b = 6, although QLS still yields a visibly broader upper tail. Numerically, the MLE mean of b decreases from 8.22493 at n = 20 to 6.17895 at n = 250, while its RMSE decreases from 4.57452 to 0.44839. The corresponding MLE mean for λ changes from 0.530447 to 0.500169. These observations agree with the reported results in Tables 3—6. Figures 6 and 7 summarize RMSE across sample sizes, and Figure 8 illustrates the composite rankings in Tables 8 and 9.

The 24-page supplementary R-graphics document reports all sample sizes (n = 20, 50, 125, 250) and all five parameters (λ, k, θ, a, b). Its parameter-specific four-panel plots comprise MLE-versus-PM sampling histograms, boxplots for all eight estimators, running means across replications, and empirical CDFs of absolute estimation error. The supplementary convergence summaries report successful numerical fits and the individual nonzero optimizer status codes. Across the supplied results, successful fits range from 99.2% to 100.0%; these rates indicate numerical termination success, not necessarily unbiased or precise breakpoint estimation. In particular, the running-mean trajectories must not be interpreted as within-run optimizer traces. All numerical tables in the manuscript are preserved, and the figures use the uploaded R output rather than newly generated synthetic data.

© 2026 NSP
Natural Sciences Publishing Cor.

6 Application to Real Data: Glass Fiber Strengths

In this section, we analyse the 63 supplied glass-fibre strength measurements for 1.5-cm fibres and compare the EWE Spliced-Bridge model with the six fitted alternatives BeE, KuE, EGE, WeE, GoE, and E. Tables 10—15 retain the original descriptive statistics, parameter estimates, likelihood criteria, goodness-of-fit statistics, and model rankings. Figures 9 and 10 show the EWE curves reconstructed from its fitted parameters together with numerical comparisons covering all seven fitted models. The original multipanel competitor curves remain in the supplementary figure archive.

The 63 measurements are from 0.55 to 2.24, with an arithmetic mean of 1.51 and median of 1.59. The fact that the mean is below the median, and the skewness coefficient of -0.88, indicate a slightly negatively skewed sample. This can be seen in the histogram: most observations are concentrated around 1.4-1.8, but there are a few smaller observations that widen the lower tail and pull the mean down. The trimmed mean of 1.54 is in between the ordinary mean and the median, which indicates that the lower observations do not have a significant impact on the center of the data.

The standard deviation is 0.32 and the coefficient of variation is about 21.51%, indicating some relative dispersion. The middle 50% of observations are in the range of 1.375-1.685 (IQR = 0.310). The excess kurtosis of 0.80 indicates that the distribution is more peaked and tail sensitive than a normal model. A flexible model that can reproduce asymmetry, clustering around the central mode, and tail behavior is also suitable for this data.

Table 10: Descriptive statistics for the 63 glass-fiber strength observations.

Statistic	Value
Number of observations (n)	63
Mean	1.51
Standard deviation	0.32
Median	1.59
Trimmed mean	1.54
Median absolute deviation (MAD)	0.16
Minimum	0.55
Maximum	2.24
Range	1.69
First quartile (Q1)	1.375
Third quartile (Q3)	1.685
Interquartile range (IQR)	0.310
Coefficient of variation	21.51%
Skewness	-0.88
Kurtosis (excess)	0.80
Standard error of the mean	0.04

The EWE model was fitted by maximum likelihood using the five-parameter vector $(\lambda, k, \theta, a, b)$. The optimization algorithm reported convergence, and the minimized negative log-likelihood was 18.73196. The corresponding maximum-likelihood estimates are $\hat{\lambda} = 2.40677$, $\hat{k} = 4.53197$, $\hat{\theta} = 1.58816$, $\hat{a} = 0.000736$, and $\hat{b} = 2.11002$.

The fitted Weibull bridge has a relatively large shape estimate ($\hat{k} \approx 4.53$) and a scale estimate $\hat{\theta} \approx 1.59$, which is close to the sample median. This is consistent with the strong concentration of observations around the central region of the histogram. The estimated left breakpoint is extremely close to zero and lies far below the smallest observed value (0.55), whereas the estimated right breakpoint is close to the upper end of the sample (2.24). Hence, under the fitted EWE structure, essentially the entire observed sample is assigned to the Weibull bridge: 62 of the 63 observations lie between $\hat{a}$ and $\hat{b}$, no observation lies in the left exponential regime, and only the largest observation (2.24) lies in the right exponential regime.

This breakpoint configuration is informative. It indicates that the central Weibull component is doing most of the empirical fitting, while the exponential tail component is used only for the extreme upper observation. The standard error for $\hat{b}$ is returned as NaN, even though the numerical optimizer reports convergence. Thus, convergence of the objective function should not be interpreted as complete inferential stability for the right breakpoint. The missing standard error is consistent with weak local identification or a nearly singular Hessian for b. For a final inferential analysis, profile likelihood or a grid/profile treatment of the breakpoints, and preferably bootstrap confidence intervals, would provide a more reliable assessment of breakpoint uncertainty.

© 2026 NSP
Natural Sciences Publishing Cor.

Table 11: Maximum-likelihood estimates and reported uncertainty measures for the EWE model.

Parameter	MLE	Std. Dev.	Lower 95% CI	Upper 95% CI
λ (tail rate)	2.4067678705	0.7188593	0.9978295	3.8157063
k (Weibull shape)	4.5319724385	0.5569785	3.4403147	5.6236302
θ (Weibull scale)	1.5881570467	0.0454961	1.4989864	1.6773277
a (left breakpoint)	0.0007363239	0.00000947	0.0007178	0.0007549
b (right breakpoint)	2.1100155457	NaN	NaN	NaN

Table 12: Information criteria for EWE and the competing models (ordered by AIC).

Model	-L	AIC	CAIC	BIC	HQIC
EWE	18.73196	47.46392	48.51655	58.17959	51.67845
BeE	23.26844	52.53687	52.94365	58.96628	55.06559
GoE	24.68107	55.36215	55.76893	61.79155	57.89087
EGE	25.57331	57.14662	57.55340	63.57603	59.67534
WeE	33.05678	72.11356	72.52034	78.54297	74.64228
KuE	33.66692	73.33384	73.74062	79.76325	75.86256
E	54.65552	111.31100	111.37660	113.45420	112.15390

Table 12 compares the EWE model with the six competing models using the minimized negative log-likelihood (-L), Akaike information criterion (AIC), corrected AIC (CAIC), Bayesian information criterion (BIC), and Hannan-Quinn information criterion (HQIC). For all of these criteria, smaller values indicate a better trade-off between empirical fit and model complexity.

The EWE model achieves the smallest value for every reported likelihood-based criterion: -L = 18.73196, AIC = 47.46392, CAIC = 48.51655, BIC = 58.17959, and HQIC = 51.67845. This result is particularly notable because EWE contains five estimated parameters and therefore receives a larger complexity penalty than several competitors. Despite this penalty, it still produces the minimum AIC, CAIC, BIC, and HQIC values, showing that the improvement in likelihood is large enough to compensate for the additional model flexibility.

The ΔAIC value of the EWE model is zero by definition. The normalized AIC weight of EWE is approximately 0.904, compared with 0.0715 for BeE, 0.0174 for GoE, and 0.0071 for EGE. Therefore, conditional on the reported fitted values, EWE receives about 90.4% of the total AIC support among the seven models and about 12.6 times the AIC support of BeE.

A useful nuance appears in the BIC comparison. The difference between EWE and BeE is only about 0.787, so BIC alone does not sharply separate these two models. However, BeE did not achieve algorithmic convergence and its empirical-distribution statistics W and A are substantially larger than those of EWE. Accordingly, the combined numerical evidence still favors EWE over BeE, while the non-convergence of BeE makes its reported optimum and information criteria less dependable.

The Cramér-von Mises statistic W, Anderson-Darling statistic A, and Kolmogorov-Smirnov (K-S) statistic quantify the discrepancy between the fitted theoretical distribution and the empirical distribution. Smaller values indicate closer agreement. EWE gives the smallest W (0.25660) and A (1.40484) values among all models, providing strong relative evidence that its fitted distribution follows the empirical distribution more closely over the full sample range and, in particular, in regions emphasized by the Anderson-Darling criterion.

For the K-S statistic, BeE has the smallest value (0.24161) and EWE is a very close second (0.24232), a difference of only about 0.00070. However, the BeE optimization did not converge, whereas the EWE optimization did. Among the models with reported convergence, EWE therefore has the smallest K-S statistic. The two models for which convergence was not achieved are BeE and WeE; their parameter estimates and model-selection measures should consequently be treated with caution.

An important distinction is required between relative fit and absolute goodness of fit. All reported K-S p-values are below 0.05. In particular, the EWE p-value is 0.001225. Thus, at the conventional 5% significance level, the K-S test rejects exact agreement between every fitted model and the empirical distribution, including EWE. Therefore, the correct conclusion is not that EWE provides a statistically perfect fit; rather, EWE provides the strongest relative fit among the reported models according to most criteria. This distinction should be retained in the final manuscript to avoid overstating the goodness-of-fit result.

© 2026 NSP
Natural Sciences Publishing Cor.

Table 13: Empirical-distribution goodness-of-fit statistics and convergence status.

Model	W	A	K-S	K-S p-value	Convergence	K-S rank
EWE	0.256601	1.404844	0.2423154	0.001224573	Converged	2
BeE	0.522921	2.831717	0.2416138	0.001278096	Not converged	1
GoE	0.553588	3.004439	0.2702232	0.0002019591	Converged	6
EGE	0.592531	3.216750	0.2676715	0.0002400883	Converged	5
WeE	0.826256	4.483202	0.2515899	0.0006875803	Not converged	3
KuE	0.850892	4.609873	0.2601410	0.0003961602	Converged	4
E	1.046695	5.610624	0.3472277	5.052056e-07	Converged	7

We summarise the fitted parameter values in Table 14. Several competing models have very large parameter estimates: $\lambda\hat{} = 73.2369$ for BeE, $k\hat{} = 24.8737$ for EGE, $\lambda\hat{} = 37.0088$ for WeE, and $k\hat{} = 38.7215$ for GoE. Large values of the fitted parameters are not necessarily invalid, but they may signal strong parameter compensation, a flat likelihood region, or numerical sensitivity. This is particularly relevant for both BeE and WeE as their optimizers were not able to converge.

Table 14: Maximum-likelihood estimates for EWE and the competing models.

Model	Maximum-likelihood parameter estimates
EWE	$\lambda = 2.40677,\ k = 4.53197,\ \theta = 1.58816,\ a = 0.000736,\ b = 2.11002$
BeE	$r = 0.201800,\ u = 73.236919,\ b = 17.220845$
KuE	$r = 2.076364,\ u = 5.797385,\ b = 2.174478$
EGE	$r = 24.873715,\ u = 0.339447,\ b = 10.658877$
WeE	$r = 7.598587,\ u = 37.008811,\ b = 2.242472$
GoE	$r = 38.721536,\ u = 0.302197,\ b = 12.097204$
E	$b = 1.790486$

Table 15 provides an overall descriptive ranking based on eight reported criteria: negative log-likelihood, AIC, CAIC, BIC, HQIC, Cramér–von Mises W, Anderson–Darling A, and the K–S statistic. Each criterion is ranked in ascending order, and the mean of the eight ranks gives the overall score. This summary does not replace individual goodness-of-fit evidence.

EWE is first overall, with an average rank of 1.125. It ranks first for -L, AIC, CAIC, BIC, HQIC, W, and A, and second only for K-S. BeE is second overall, but its lack of convergence undermines confidence in that result. GoE and EGE are the next top two, while WeE and KuE are less competitive. The single parameter E model is clearly the weakest according to all major numerical criteria.

Figure 9 combines the fitted EWE density and the empirical glass-fibre histogram with a direct seven-model ΔAIC comparison computed from Table 12. This presentation preserves the full numerical model comparison without assuming unreported parameterizations for the competing fitted curves. The original multipanel fitted-density images are retained in the supplementary graphical archive.

Figure 10 contrasts the empirical CDF with the reconstructed EWE CDF and displays the reported K–S statistics for all seven models. The point symbols distinguish fits that converged from those that did not. The EWE CDF is calculated from its stated equation and fitted parameters; curves for the other six models are not recomputed because their complete functional specifications are not supplied in the manuscript.

Combined with the likelihood, information criteria, empirical-distribution statistics, convergence diagnostics and the graphical results we have shown, EWE is the strongest of all reported alternatives for this data. It has the smallest negative log-likelihood and all four information criteria and the smallest Cramér-von Mises and Anderson-Darling statistics. Its K-S statistic is in fact close to BeE and the best of the models with numerical convergence. We also have a clear structure for the fitted EWE. The estimated bridge scale $\theta\hat{} = 1.588$ is very close to the centre of the sample while $k\hat{} = 4.532$ is a relatively dense central density. At the same time the estimated breakpoints indicate that the central bridge dominates almost the entire empirical range. This makes the EWE model highly adaptive for the present dataset, but also means that the breakpoint uncertainty should be studied more carefully before strong inferences are made about the separate tail regimes.

© 2026 NSP
Natural Sciences Publishing Cor.

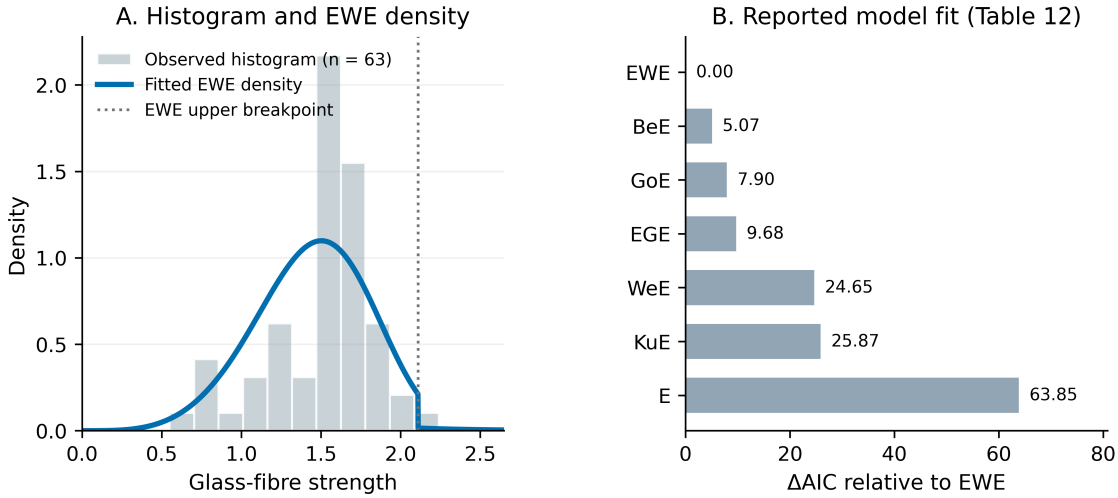

Fig. 9: (A) Glass-fibre histogram and fitted EWE density (blue solid; n = 63), with the estimated upper breakpoint (grey dotted). (B) ΔAIC values for all seven fitted models, calculated from Table 12; smaller values indicate greater relative AIC support.

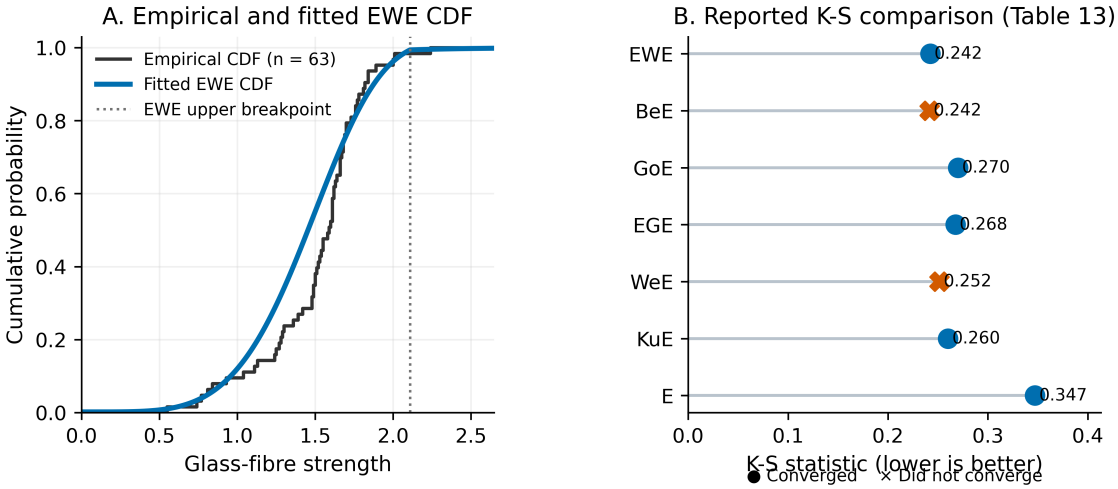

Fig. 10: (A) Empirical CDF of the 63 observations (black step), fitted EWE CDF (blue solid) and estimated upper breakpoint (grey dotted). (B) Reported K–S values for all seven models from Table 13; crosses identify optimization non-convergence.

© 2026 NSP
Natural Sciences Publishing Cor.

Table 15: Descriptive overall ranking based on the eight reported fit criteria.

Overall position	Model	Average rank	AIC weight	Convergence
1	EWE	1.125	0.903898	Converged
2	BeE	1.875	0.071539	Not converged
3	GoE	3.375	0.017420	Converged
4	EGE	4.125	0.007138	Converged
5	WeE	4.750	0.000004	Not converged
6	KuE	5.750	0.000002	Converged
7	E	7.000	0.000000	Converged

The numerical advantage of EWE should therefore be stated as a relative-model result: EWE is the best-performing candidate among the models considered under the reported fitting procedure. It should not be described as passing an absolute K-S goodness-of-fit test, because its K-S p-value is below 0.05. A rigorous manuscript can strengthen the empirical analysis by reporting profile-likelihood or bootstrap uncertainty for a and b, repeating the optimization from multiple starting values, and confirming that the final likelihood is stable across alternative optimizers.

The real-data analysis of 63 glass-fiber strength observations shows the competitive performance of the EWE Spliced-Bridge distribution. Among the 7 fitted models, EWE has the smallest negative log-likelihood (18.73196), AIC (47.46392), CAIC (48.51655), BIC (58.17959), HQIC (51.67845), and smallest Cramér-von Mises (0.25660) and Anderson-Darling (1.40484) statistics. The minimum EWE K-S statistic (0.24232) is nearly the same as that obtained by BeE (0.24161), but BeE cannot match the distribution on the graph. EWE density captures the most concentration of the observations in the center, and the cumulative curve is a bit closer than the other competitors. The observed breakpoints show that the Weibull bridge covers nearly the entire observed sample, which indicates that the proposed bridge is adaptive. Although the K-S p-value is still below 0.05 and therefore not a proper absolute fit, the overall evidence of likelihood-based selection, empirical-distribution criteria, convergence, and the graphical representation of the EWE is that this is the strongest relative model of those considered in this study.

7 Conclusion

Our new Spliced-Bridge family of continuous distributions is a combination of a central bridge distribution and common tail behavior based on continuous CDF construction. Our EWE model demonstrates the versatility of this approach by combining exponential tails with a Weibull bridge and two estimable breakpoints. We explored eight estimation procedures in simulation. We found that PM is best for small samples, and MLE is the best overall estimator for larger samples. With increasing sample size, MPS is still very competitive for some parameters. The decreasing bias, MSE, and RMSE with increasing sample size show that our estimation is more accurate and stable. The real data analysis also showed that the EWE model has the best relative performance among the fitted competitors. In general, the family presented is a good model for modeling heterogeneous distributions, although breakpoint estimation may require careful calculation.

Acknowledgment

The authors extend their appreciation to Umm Al-Qura University, Saudi Arabia for funding this research work through grant number: 26UQU4300206GSSR06.

Funding Statement

This research work was funded by Umm Al-Qura University, Saudi Arabia under grant number: 26UQU4300206GSSR06.

Appendix A

For reproducibility, the 63 observations used in the analysis are listed below in the same numerical form supplied for the R application.

© 2026 NSP
Natural Sciences Publishing Cor.

Table A1: The 63 glass-fiber strength observations.

0.55	0.74	0.77	0.81	0.84	1.24	0.93
1.04	1.11	1.13	1.30	1.25	1.27	1.28
1.29	1.48	1.36	1.39	1.42	1.48	1.51
1.49	1.49	1.50	1.50	1.55	1.52	1.53
1.54	1.55	1.61	1.58	1.59	1.60	1.61
1.63	1.61	1.61	1.62	1.62	1.67	1.64
1.66	1.66	1.66	1.70	1.68	1.68	1.69
1.70	1.78	1.73	1.76	1.76	1.77	1.89
1.81	1.82	1.84	1.84	2.00	2.01	2.24

References

[1] A. M. Abd El-latif, F. A. Almulhim, N. A. Noori, M. A. Khaleel and B. S. Alsaedi, Properties with application to medical data for new inverse Rayleigh distribution utilizing neutrosophic logic, J. Radiat. Res. Appl. Sci., **18**, 101391 (2025).

[2] I. Abubakar Sadiq, S. I. S. Doguwa, A. Yahaya and A. Usman, Development of new generalized odd Fréchet-exponentiated-G family of distribution, UMYU Sci., **2**, 169–178 (2023).

[3] A. Z. Afify, E. A. Elsherpieny, A. M. El-Sheikh and G. M. Cordeiro, A generalized flexible family: theoretical properties, estimation, and risk analysis, Benha J. Humanit. Sci., **5**, 431–465 (2026).

[4] A. A. H. Ahmadini, B. Elkalzah, K. Elsharkawy and G. A. Marei, Reliability estimation of *s*-out-of-*k* systems under inverted Z-Lindley stress-strength models with progressive censoring: an engineering application, Qual. Reliab. Eng. Int., (2026), https://doi.org/10.1002/qre.70391.

[5] A. A. H. Ahmadini, M. Elwahab, M. Elgarhy, H. Aljohani and G. A. Marei, Modulating early-life risk without breaking Weibull structure: an odds-based Weibull model for engineering failure-time data, Rev. Int. Métodos Numér. Cálc. Diseño Ing., **42**(6), (2026), https://doi.org/10.23967/j.rimni.2026.10.82546.

[6] E. E. Akarawak, S. J. Adeyeye, M. A. Khaleel, A. F. Adedotun, A. S. Ogunsanya and A. A. Amalare, The inverted Gompertz-Fréchet distribution with applications, Sci. Afr., e01769 (2023).

[7] A. H. Alenezy, B. Elkalzah, A. F. I. Alahshan and G. A. Marei, Robust inference for stress-strength reliability of the Garhy distribution under diverse record schemes with engineering and medical applications, Mathematics, **14**, 1940 (2026).

[8] A. H. Alenezy, K. A. Rashedi, A. B. Ghorbal and G. A. Marei, Bridging Markov chain Monte Carlo techniques and Tierney–Kadane approximations for progressively censored Garhy reliability models: simulation insights and a medical application, Mathematics, **14**, 1777 (2026).

[9] A. H. Alenezy, L. S. Diab, K. A. Rashedi and G. A. Marei, Inference for a step-stress model under the inverted Z-Lindley distribution with progressive Type-II censoring, AIMS Math., **11**, 31919–31962 (2026).

[10] H. M. Aljohani, F. M. Zaghdoun, M. A. Meraou et al., A novel extension of the exponential distribution with application in modeling complex lifetime and environmental data, Sci. Rep., **15**, 33581 (2025).

[11] A. Alzaatreh, C. Lee and F. Famoye, A new method for generating families of continuous distributions, Metron, **71**, 63–79 (2013).

[12] T. W. Anderson and D. A. Darling, Asymptotic theory of certain goodness-of-fit criteria based on stochastic processes, Ann. Math. Stat., **23**, 193–212 (1952).

[13] C. Chesneau, Theory on a new bivariate trigonometric Gaussian distribution, Innov. Stat. Probab., **1**, 1–17 (2025).

[14] K. Cooray and M. M. A. Ananda, Modeling actuarial data with a composite lognormal-Pareto model, Scand. Actuar. J., **2005**, 321–334 (2005).

[15] G. M. Cordeiro and M. de Castro, A new family of generalized distributions, J. Stat. Comput. Simul., **81**, 883–898 (2011).

[16] H. Cramér, On the composition of elementary errors, Scand. Actuar. J., **1928**, 13–74 (1928).

[17] S. Efromovich, Quasi-linear wavelet estimation, J. Amer. Statist. Assoc., **94**, 189–204 (1999).

[18] B. Elkalzah, M. O. Mohamed, K. Elsharkawy, E. S. Osman, A. Aldukeel and G. A. Marei, Classical and Bayesian estimation of stress-strength reliability under the discrete alpha-power Weibull distribution with incomplete and record data: application to high-voltage capacitors, AIMS Math., **11**, 6374–6399 (2026).

[19] M. A. Eltehiwy and N. A. T. AbuEl-magd, A new transformation to reduce skewness in data with bounded support, Mod. J. Stat., **2**, 100–111 (2026).

[20] N. Eugene, C. Lee and F. Famoye, Beta-normal distribution and its applications, Commun. Stat. Theory Methods, **31**, 497–512 (2002).

[21] A. M. Gemeay, T. Moakofi, O. S. Balogun, E. Ozkan and M. M. Hossain, Analyzing real data by a new heavy-tailed statistical model, Mod. J. Stat., **1**, 1–24 (2025).

[22] K. H. Habib, M. A. Khaleel, H. Al-Mofleh, P. E. Oguntunde and S. J. Adeyeye, Parameters estimation for the [0,1] truncated Nadarajah-Haghighi Rayleigh distribution, Sci. Afr., e02105 (2024).

[23] H. H. Hassan, G. M. Cordeiro and A. Z. Afify, The new Marshall-Olkin Lomax distribution: properties and estimation, Benha J. Humanit. Sci., **5**, 494–517 (2026).

© 2026 NSP
Natural Sciences Publishing Cor.

[24] M. Imran, M. A. F. Elbarkawy, F. Jamal and G. A. Marei, An extended Lindley model with applications to entropy-based loss and actuarial risk measures, Comput. J. Math. Stat. Sci., **5**, 1–33 (2026).
[25] H. S. Klakattawi, Survival analysis of cancer patients using a new extended Weibull distribution, PLoS ONE, **17**, e0264229 (2022).
[26] S. A. Klugman, H. H. Panjer and G. E. Willmot, Loss Models: From Data to Decisions, Wiley, New York, (1998).
[27] N. Lazri and A. Sakri, Novel two parameter distribution: properties, simulation and application in interactive data analysis and finance, Asia Pac. J. Math., **12**, 47 (2025).
[28] A. W. Marshall and I. Olkin, A new method for adding a parameter to a family of distributions with application to the exponential and Weibull families, Biometrika, **84**, 641–652 (1997).
[29] M. Matuszczak, M. Żbikowski and A. Teodorczyk, Predictive modelling of turbofan engine components condition using machine and deep learning methods, Eksploat. Niezawodn., **23** (2021).
[30] N. A. Noori, M. A. Khaleel, T. M. Alharigy, E. M. Almetwally and M. Elgarhy, The neutrosophic Gompertz-G family: analytical properties, simulation studies, and applications to real data, Mod. J. Stat., **2**, 75–99 (2026).
[31] A. N. Nooruldeen, A. K. Mundher and D. A. Dalya, The modified Burr-III distribution properties, estimation, simulation, with application on real data, Iraqi Stat. J., Special Issue ICSA2025, 225–246 (2025).
[32] G. O. Orji, H. O. Etaga, E. M. Almetwally, C. P. Igbokwe, O. C. Aguwa and O. J. Obulezi, A new odd reparameterized exponential transformed-X family of distributions with applications to public health data, Innov. Stat. Probab., **1**, 88–118 (2025).
[33] K. A. Rashedi, L. S. Diab, A. H. Alenezy and G. A. Marei, A one-parameter decreasing-hazard lifetime model with exact inference on a bounded-below support, AIMS Math., **11**, 24445–24489 (2026).
[34] K. A. Rashedi, L. S. Diab, A. H. Alenezy and G. A. Marei, Inference for stress-strength reliability under unified hybrid censoring: a one-parameter model with applications, Mathematics, **14**, 2041 (2026).
[35] H. M. Reyad, M. Alizadeh, J. Farrukh, S. Othman and G. G. Hamedani, The exponentiated generalized Topp-Leone-G family of distributions: properties and applications, Pak. J. Stat. Oper. Res., **15**, 1–24 (2019).
[36] A. M. Salih, S. Khalaf, K. N. Abdullah and N. A. Noori, Neutrosophic extension of the new odd Weibull-inverse Weibull distribution: theory and applications, F1000Research, **14**, 1454 (2025).
[37] D. P. M. Scollnik, On composite lognormal-Pareto models, Scand. Actuar. J., **2007**, 20–33 (2007).
[38] Z. Shah, D. M. Khan, Z. Khan, N. Faiz, S. Hussain, A. Anwar, T. Ahmad and K.-I. Kim, A new generalized logarithmic-X family of distributions with biomedical data analysis, Appl. Sci., **13**, 3668 (2023).
[39] H. Sharqa, M. Ahsan-ul-Haq, J. Zafar and M. A. Khaleel, Unit Xgamma distribution: its properties, estimation and application, Proc. Pak. Acad. Sci. A, **59**, 15–28 (2022).
[40] Q. Xia, Y. Tsong and Y. T. Weng, Methods and applications of percentile estimation, J. Biopharm. Stat., **30**, 267–276 (2020).

© 2026 NSP
Natural Sciences Publishing Cor.